Invited Paper: SPIE 4008-70 06 March 2000 LBNL-45277

Recent progress on CCDs for astronomical imaging

D. E. Groom
Lawrence Berkeley National Laboratory, Berkeley, CA 94720

"Don't let any photons fall onto the floor!"
. . . Anon.

ABSTRACT

We review recent progress in the field, using as a framework a partial list of present limitations and problems: CCD and mosaic size, packing fraction in mosaics, red response and fringing, and intrinsic point-spread function due to lateral charge diffusion. Related topics such as orthogonal-transfer CCDs and the special requirements of adaptive-optics wavefront sensors are also discussed. Only cursory attention is given to other relevant issues, such as readout speed and anti-blooming techniques.

Keywords: CCD, mosaic, high resistivity, fully depleted, PSF, astronomical, fringing, Lawrence Berkeley National Laboratory, Lick Observatory

1. INTRODUCTION

On 1936 March 26, a special train began its 14-day journey from Corning, New York, to Pasadena, California, carrying the 200-inch mirror blank destined for Mt. Palomar as its only cargo. Thousands, including entire school classes, made the pilgrimage to the tracks to witness its passing.[1] Before and after the "Giant Eye" on Palomar was built, public interest has attended the construction of the great telescopes, although with less attention than was accorded to such an upbeat event during the depths of the Great Depression (and with the help of the Caltech publicity machine).

By contrast, a far more significant advance in astronomy came unheralded and generally unnoticed, with the introduction of the CCD in 1976.[2] With 30–100 times the sensitivity of photographic plates, the CCD gave every 1-m telescope the reach of Palomar. In contrast to the limited linear range of photographic emulsions, its linear response for the first time allowed astronomers to look at objects far fainter than the sky. The output was already digital. Together, these features extend the reach of optical astronomy to a large fraction of the observable universe.

As of 1974, image intensifiers were emerging as a competitor to photographic plates. Both were rapidly replaced by CCDs after visits to observatories by JPL's Traveling CCD Camera System overcame astronomers' reticence. The

deg@lbl.gov, http://ccd.lbl.gov

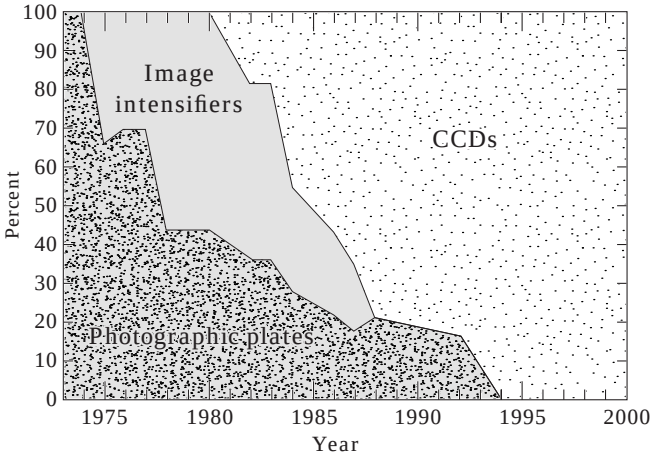

Figure 1. The demography of optical sensitive area devoted to observation at the European Southern Observatory, 1973–2000. Data were collected and plotted by G. Monnet (ESO), and shown here with his permission.

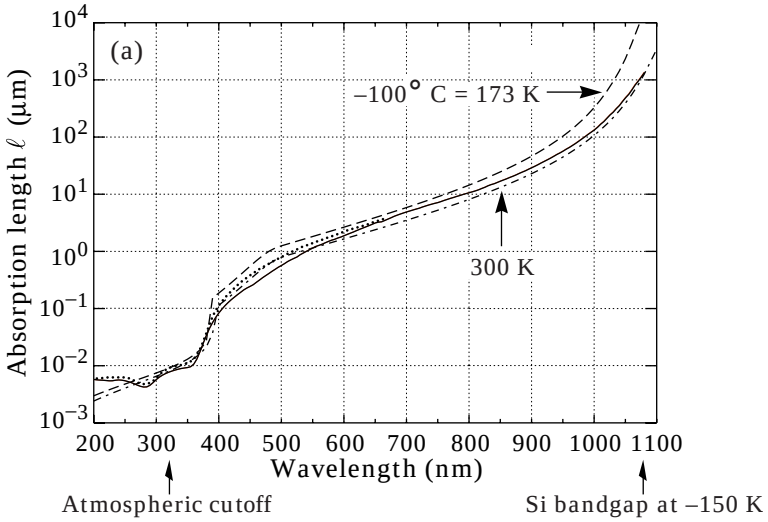

Figure 2. Absorption length of light (intensity, not amplitude) ℓ in silicon. Measurements at room temperature (300 K) are shown by the solid curve.[3,4] The dashed curves are calculated from the phenomenological fits by Rajkanan *et al.*[5]

history of optical sensitive area observed via the different technologies at the European Southern Observatory (ESO) is shown in Figure 1, which was provided by G. Monnet.

CCDs are among the largest integrated circuits being manufactured,* but they are still tiny compared with the 14-inch square area plates used in the Palomar 48-inch Schmidt telescope. Accordingly, much effort has gone into making larger CCDs and mosaics of many CCDs.

The challenge of designing a device sensitive to light from the atmospheric cutoff, at about 320 nm, to just short of the silicon bandgap, just above 1000 nm, is evident from Figure 2. Over this range, the absorption length of light changes by more than four orders of magnitude! On the blue end, light is absorbed by the gate structure on the front of a CCD, leading to the use of "thinning" (removing all the substrate, leaving only the epitaxial layer) and rear illumination. Even so, field inversion near the back surface of a thinned CCD leads to the loss of electrons produced near this surface, giving rise to a variety of heroic measures to maintain the blue sensitivity.

Red light causes different problems. Redward of about 600 nm the gate structure is essentially transparent, so that front illumination would be practical if only red and near-infrared were to be observed. However, only the epitaxial layer, typically 20 μm thick, is sensitive, and it in turn becomes transparent for $\lambda \gtrsim 800$ nm. In the case of a front-illuminated CCD, e/hole photoproduction then occurs in the low-resistivity substrate, where most of the charge recombines. Back illumination introduces a new problem, since in general the light undergoes multiple reflections before being absorbed with consequent charge collection, or escape through one of the surfaces. The familiar interference fringes create problems, and under their presence indicates low quantum efficiency (QE) as well. Model calculations of QE for thin and thick CCD are shown in Figure 3(a).

In general, the charge produced near the back surface of a CCD must diffuse through a field-free region before encountering electric fields which rather quickly transport it to the potential wells. The consequent lateral diffusion leads to an intrinsic point spread function (PSF) which can be troublesome or unacceptable.

All of these problems are being addressed by CCD manufacturers, government laboratories, and researchers at observatories, and hence provides a reasonable framework in which to discuss recent progress in the field. Outside this framework but also covered are a number of developments which deserve special mention: The orthogonal transfer CCDs being developed by MIT/Lincoln labs in cooperation with J. Tonry,[7,8] and the small but very fast CCDs needed for adaptive optics (AO) systems.

*The Philips 7k×9k CCD packaged at Steward Observatory has about 50 times the area of a Pentium II chip.

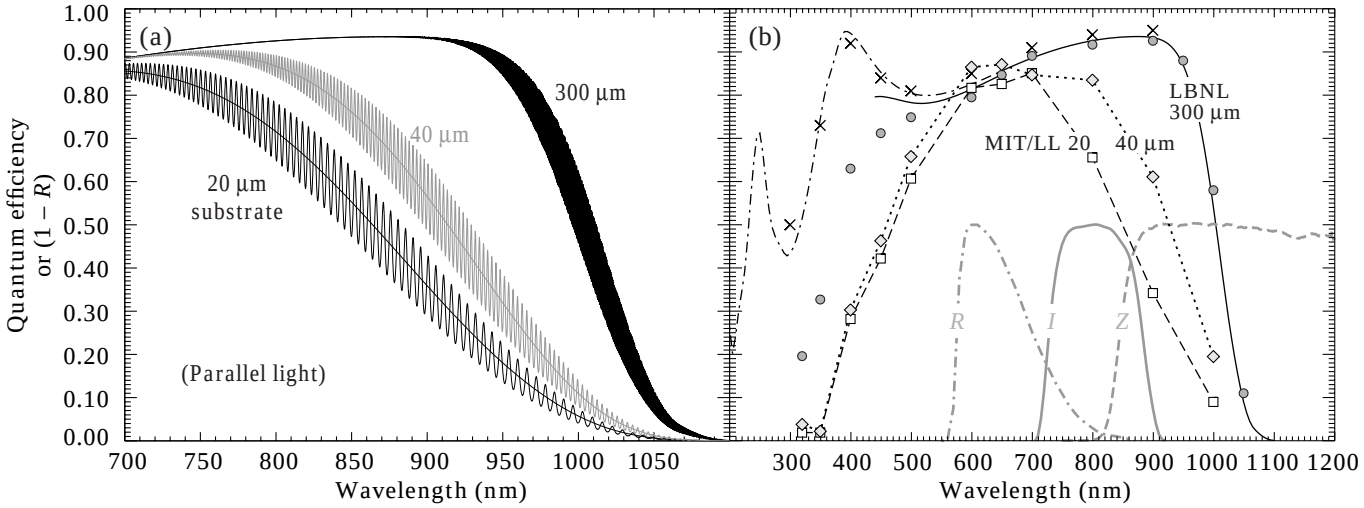

Figure 3. (a) Modeled quantum efficiencies for CCDs thinned to 20 and 40 μm, and for a totally depleted CCD on a high-resistivity 300-μm substrate. For typical nonparallel light the fringing is reduced in the thinned CCD and becomes negligible in the thick CCD.[6] (b) Measured (circles) and modeled QE for a UC/LBNL totally-depleted CCD with a red-optimized AR coating. Expectation (dot-dashed curve) and measurements ($\times$'s) of $(1-R)$, where R is the reflectivity, are also shown. For comparison, Lick Observatory QE measurements for 20 and 40 μm depletion region MIT/Lincoln Lab CCDs are shown. The normalization of their measurements is possibly uncertain, and these particular CCDs have an atypically low blue response because of a one-layer AR coating. Unnormalized broadband filter responses are indicated in gray.

2. LARGER CCDS AND LARGER ARRAYS

The 1976 JPL traveling CCD camera contained one 400×400 CCD, later upgraded to a TI 512×512 $(15\ \mu\mathrm{m})^2$ backside illuminated chip. By 1990 2k×2k CCDs were available. Until mid-1996 a Tektronix 2k×2k $(24\ \mu\mathrm{m})^2$ was the best imager available at the CTIO 4-m telescope, although mosaic cameras had appeared as early as 1992. The Big Throughput Camera (BTC), consisting of four widely-spaced SITe chips of this kind, replaced it at this time. Since then, the 2k×4k $(15\ \mu\mathrm{m})^2$ CCD has become a sort of (astronomical) industry standard, and forms the basic unit of most recent mosaic cameras. These CCDs are obtained from SITe, Marconi Applied Technologies (nee EEV), MIT/Lincoln Labs, and perhaps others; they will soon be supplied by Hamamatsu and Sarnoff as well.

G. Luppino has observed that the number of pixels in the largest camera increases by a factor of about 1.4 per year, corresponding to a factor of 28 per decade. The intercept at 1990 is at 5×10^6 pixels, slightly more than the 2000×2000 actually available at the time. He further observes that if the present trend continues, the largest camera will cover the earth after little more than another century of development.[†]

The University of Hawaii 4k×4k mosaic camera was commissioned in 1992, and a sequence of ever-larger arrays has followed since. A tentative summary of large CCD arrays commissioned since about 1999 is given in Table 1. At least four 8k×8k devices were in use prior to 1998, starting with the University of Hawaii 8k×8k camera at CFHT in 1995, and there are now 11 cameras with this format. The CFH12K (see Fig. 4) and Sloan Digital Sky Survey camera are presently the largest in operation, although they are quite different in concept and purpose. Three close-packed arrays in the 16k×16k to 18k×18k class should be in operation within 2–3 years.

More speculative are a number of proposed cameras for ground and space telescopes. One of the more adventurous of these projects is the Wide-Field High-Resolution Optical Imaging (WFHRI) array proposed by Kaiser, Tonry, and Luppino.[9] Data from an array of perhaps twenty-five 1.5 m telescopes is combined. Each has an 1800×1800 array

[†]In high-energy physics a similar exponential growth in center-of-mass energy, by a factor of roughly 10 per decade, is often shown by the famous "Livingstone plot." This trend has continued since the early days of the cyclotron in the 1930's. Moore's Law for semiconductors provides another example.

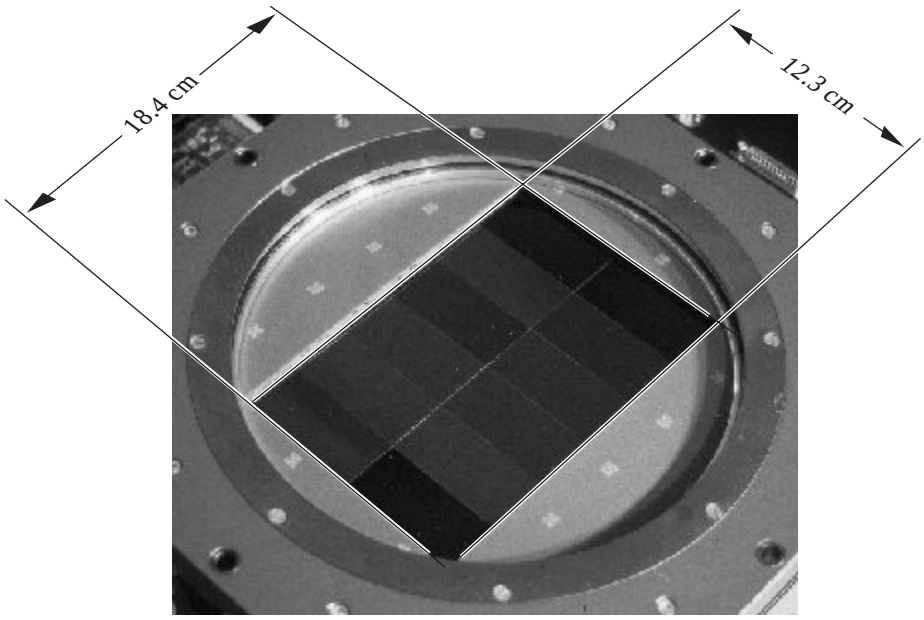

Figure 4. The CFH12K mosaic, presently in use at the 3.6 m Canada-France-Hawaii Telescope.

of 600×600 (5 μm)^2 pixel orthogonal transfer CCDs (OTCCDs,[7,8] discussed below). Wherever they occur, bright stars are used as guides for charge shifting to correct for the effects high-altitude air turbulence in nearby CCDs.

The Supernova Cosmology Project is framing a proposal for a dedicated SuperNova/Accleration Probe (SNAP) satellite, which plans use of the UC/LBNL totally-depleted CCDs to obtain the red response needed to observe objects at cosmological distances. The present concept calls for 10^9 $\lesssim$10 μm pixels, or $\approx$ 250 2k×2k CCDs.

The ground-based Dark Matter Telescope (DMT; `dmtelescope.org`) and the space-based Global Astrometric Interferometer for Astrophysics (GAIA)[10] project have similar ambitions.

It is our understanding that 4-side abutment schemes are also being developed at Steward Observatory and other places.

2.1. Packing fraction and four-side abutment

Since several images are usually combined to eliminate cosmic rays and CCD cosmetic difficulties, dithering to eliminate cracks between CCDs in the final image is not a serious problem. However, in the interest of efficiency and convenience, close-packing of the CCDs is desirable. In most of the present mosaic arrays, packing fractions in excess of 95% are achieved using 3-side abutment. This generation of CCDs has an umbilical on the 4th side, making close abutment on all four sides difficult or impossible.

This problem has received considerable attention, with the result that several 4-side abutable packages are available or are being developed. Marconi Applied Technologies (MAT, nee EEV) offers an impressive package in which the end connections are "wrapped under" to a ZIF connector on one end of the bottom (CCD front side), as shown in Fig. 5(a) and (b). A combination of indexing pins and insertion guide rods permits nearly idiot-proof insertion between close neighbors.

A MIT/LL design is shown in Fig. 5(b). It is similar in concept, although in this case there are bonding pads on both sides of the CCD and hence a connector on each end. This particular design is for the WFHRI detector discussed above.

Of necessity, the UC/LBNL totally-depleted CCD has connection pads on the "wrong side," i.e. the blind front side bonded to the package. In the design being developed, the two contact-pad ends of the CCD cantilever from the edges of an aluminum nitride circuit card to which the front side of the CCD is cemented. Wire bonds jumper from the CCD pads to the circuit card, and external connections are then made via a central flex-cable connector which

Table 1. CCD mosaic arrays commissioned since 1998.5. Four 8k×8 arrays and a number of smaller arrays saw first light earlier. Gaps indicate lack of information. To the best of our knowledge, all of the CCDs are back-illuminated except (temporarily) for those in MAGNUM.

First light	Camera	Format	Pixel size	Packing fraction	Format	Manufacturer or part number	Telescope
1998	CFH12K	12k×8k	15 μm	98%	12×(2k×4k)	MIT/LL CCID20	CFHT
1999	Suprime-Cam	10k×8k	15 μm	96.5%	10×(2k×4k)	SITe+MIT/LL*	SUBARU
1999	SDSS	12k×10k	24 μm	$\approx$ 43%	30×(2k×2k)	SITe	Apache Pt
1999	NOAO	8k×8k	15 μm	98%	8×(2k×4k)	SITe	CTIO 4-m
2000	DEIMOS	8k×8k	15 μm	97%	8×(2k×4k)	MIT/LL CCID20	Keck
2000	MAGNUM	4k×8k	15 μm	96%	4×(2k×4k)	Hamamatsu	2 m, Haleakala
2000	WFI	8k×8k	15 μm	95.9%	8×(2k×4k)		MPG/ESO
2001	UW				20×(2k×4k)?		ARC 3.5 m
2002	OmegaCAM	16k×16k		$\geq$ 80%	32×(2k×4k)		VST
2002	MegaPrime	$\geq$16k×18k	13–15 μm	> 90%	$\geq$ 36×(2k×4k)		CFHT
2002	Megacam	18k×18k	13.5 μm	> 90%	36×(2k×4.5k)	EEV CCD42-90	SAO/MMT
2004†	DMT	Annulus	13 μm		1300×(1k×1k)		DMT 8-m
2004†	WFHRI_1‡	36k×36k	5 μm		4×(30×30)×(600×600)	MIT/LL	≈25×2.5 m
2006†	SNAPsat	$\approx 10^9$ pix	15 μm	83%	$\approx$ 250×(2k×2k)	LBNL**	Satellite
2010†	GAIA	$\approx 10^9$ pix	9 μm×27μm	86%	$\approx$ 240 CCDs		ESA satellite

* Presently 4 SITe ST-002A and 4 MIT/LL CCID-20. Will add two more MIT/LL to make full array.

‡ Proposed.

† This is for the focal plane in one of ∼25 telescopes in the WFHRI array. Each array consists of 4 chips, each a 30×30 array of 600×600 OTCCDs.

** Commercial foundry licensed by LBNL.

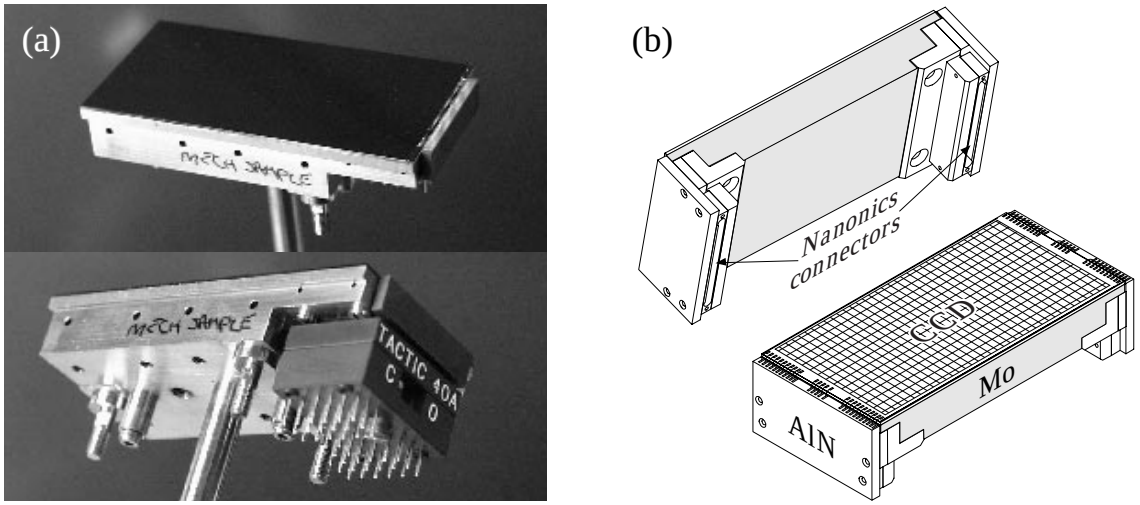

Figure 5. (a) Marconi Applied Technologies abutable CCD package for their CCD44-82 (2k×4k) and CCD42-90 (2k×4.5k) devices. In the case of the CCD42-90, the CCD/footprint area ratio is about 90%. Photos courtesy of P. R. Jordan, MAT. (b) MIT/LL developmental package for the OTCCD array discussed elsewhere, courtesy of B. E. Burke, MIT/LL.

fits into a slot in the mounting plate. Indexing pins and temporary mounting rods are similar to those in the MAT design. Wirebonding to the cantilevered chip is routinely used in a simpler package being used for characterization measurements.

However, the depletion thickness must be brought gracefully to zero before the saw-cut edge is reached, and simple electrostatics dictates that this will take place over at least a wafer thickness. This additional edge means a wider edge than on conventional CCDs. It is presently estimated that the packing fraction for the existing 2k×2k chips will be 83%, including a 250 μm gap on all sides.

2.2. Huge CCDs

Very large-area CCDs provide another approach to large-area detectors. M. Lesser's group at Steward Observatory has described the packaging and characterization of a front-illuminated Philips 7k×9k CCD with 12 μm pixels,[11] with a total photosensitive area of $86.0 \times 110.6\,\mathrm{mm}^2$. Full-wafer CCDs have also been made by Lockheed-Martin (nee Loral).[12] Their CCD, developed primarily for reconnaissance, has 9216^2 8.75 μm pixels, for a total of 85 Mpixels in a 81 mm square. It is front illuminated, and can be read out faster than 1 frame/s with less than < 25 e$^-$ rms noise.

3. THE RED PROBLEM

Thinned CCDs of necessity evoke the two-faced red devil of low QE and fringing. If the absorption length is ℓ at a particular wavelength and the sensitive region is d (typically 20 μm), the a fraction of the light $(1-e^{-d/\ell})$ is absorbed on the first pass. For a 20 μm substrate this decreases from 25% at 700 nm to 51% at 800 nm. Moreover, the light which is not absorbed will multiply reflect until it is absorbed or escapes, resulting in the familiar fringing.

This situation is shown in Fig. 3(a) for 20, 40, and 300 μm completely sensitive substrates. Although an unrealistic Si-air interface was assumed on the front (gate) side, the average QE in the fringe regions agrees well with measurements.[6] The fringes are 15 times closer in the thick CCD case. For typical non-parallel light the fringing is reduced in the thinned CCD case and is negligible for the thick CCD.

The problem is also evident in the Keck low-resolution imaging spectrometer (LRIS) quartz lamp spectrum shown in Fig. 6. Note the "sweet spot" around 910 nm.

The decreased QE is an irreducible consequence of the thickness, but can something be done to decrease fringing? SITe[13] and MAT[14] have found effective solutions to the problem. Their methods are proprietary, but a number of approaches follow from physical considerations:

- Choose the AR coating to be essentially 100% transmitting in the red region where fringing is to be eliminated. This can be done with a 1/4 wave coating with a refractive index of about 1.9. This solution has the advantage that light reflected once from the front surface can be absorbed, enhancing the QE relative to one-pass absorption. While the SITe process is not known to us, the sweet spot at 910 nm in the LRIS quartz lamp spectrum could be the result of such a coating.
- A high-index absorptive coating (a "black" dielectric) in optical contact with the front surface would prevent reflection of the light after the first pass through the CCD.
- Arrange for reflection from some part of the front surface stepped on a subpixel scale by the appropriate amount (≈ 125 nm) to kill reflected light by destructive interference.

Finally, what can be done to extend the red response? Here the physics offers one option: The sensitive region must be thicker. If the AR coating is optimal one-pass absorption more or less determines the QE at a given wavelength, and so the thickness required to reach a given wavelength may be read from Fig. 2. The silicon bandgap at just over 1000 nm provides the practical limit.

MIT/LL delivers CCDs with high-resistivity p-type silicon epitaxial layers, thinned to 40 μm. In principle this should displace the right side of the QE curve by about 50 nm, as shown in Fig. 6(a). Lick measurements of normal and high-resistivity MIT/LL CCID20 chips, shown in Fig. 3(b), indicates adequate agreement with the model prediction.

The UC/LBNL CCD is 300 μm thick, equal to the absorption length of 995 nm light at -100° C. At this wavelength, and with the present red-optimized AR coating, the modeled QE is 58%, in close agreement with measurement. (See Fig. 3(b).)

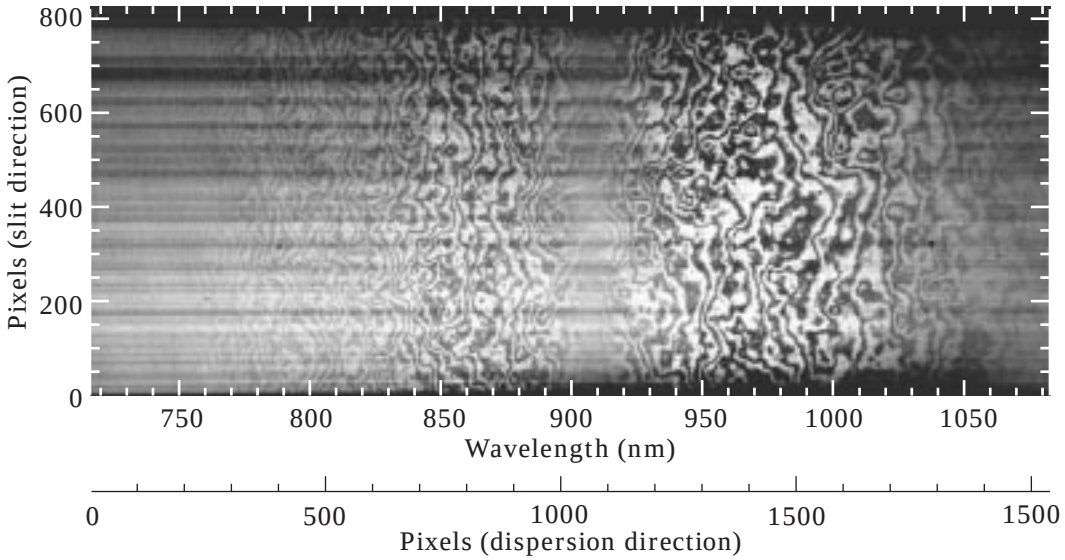

Figure 6. Quartz lamp flat obtained with the Keck Observatory low-resolution imaging spectrometer (LRIS) with the "new" SITe CCD. The image has been enhanced to emphasize the interference fringe pattern. Note the "sweet spot" near 910 nm, presumably due to $\approx 100\%$ reflectivity at this wavelength.

If the absorption length is sufficiently long that surface effects are not important (greater than a few μm) and sufficiently short that most light is absorbed on the first pass (1/4 the sensitive region thickness for 98% absorption), then essentially all of the light transmitted by the AR coating photoproduces collected charge. In this region we should find QE $= (1 - R)$, where R is the reflectivity. Reflectivity measurements thus provide a useful check on the normalization of QE measurements in this wavelength region. Such data are shown by the $\times$'s in Fig. 6(b), along with expectation (dot-dashed curve).

4. TRANSVERSE DIFFUSION: POINT-SPREAD FUNCTION AND MTF

The potential distribution as a function of distance from the front of a CCD depends on a large number of factors: channel thickness and dose, substrate doping, substrate resistivity, etc. To generate Fig.7, S. E. Holland assumed typical values for most of the parameters, treating only the resistivity of the substrate (epitaxial layer) resistivity as a free parameter. Collection mode is assumed. The potential goes to zero (linear electric field goes to zero) at some finite distance from the rear surface, as it must to avoid excessive leakage. As a result, charge produced near the back surface diffuses in the field-free region until it enters the depleted region and is swept to the potential wells. In most practical cases transverse diffusion in the field-free region dominates transverse diffusion in the depleted region, and can seriously degrade the point-spread function (PSF), or, equivalently, the corresponding modulation transfer function (MTF). The lateral distribution is known analytically;[15] it has tails substantially higher than does a Gaussian. With charge reflection at the rear surface, photon absorption close to the rear surface, and negligible surface recombination, the Fourier transform (MTF) in a field-free region of thickness L is $(\sqrt{2\pi}\cosh 2\pi f L)^{-1}$, where f is the spatial frequency.[16] (The MTF of a Gaussian PSF is also a Gaussian.)

The rms width of the field-free component of the PSF, as projected onto a transverse coordinate, is identically equal to the thickness of the field-free region.[16] For example, for a substrate 20 μm thick with a bulk resistivity of 40 Ω-cm, the 9 μm field-free region implies a 9 μm contribution to the projected PSF, or a full-width at half-maximum of 21 μm.

The field-free thickness varies a fair amount among CCDs used for astronomy, with the result that unacceptable halation sometimes occurs. For this reason this intrinsic CCD PSF has recently received considerable attention, and a number of ways to minimize its width have been explored. For a thinned CCD the only feasible solution is to arrange either the thickness or the resistivity to be such that the field-free region is as thin as possible—but not zero.

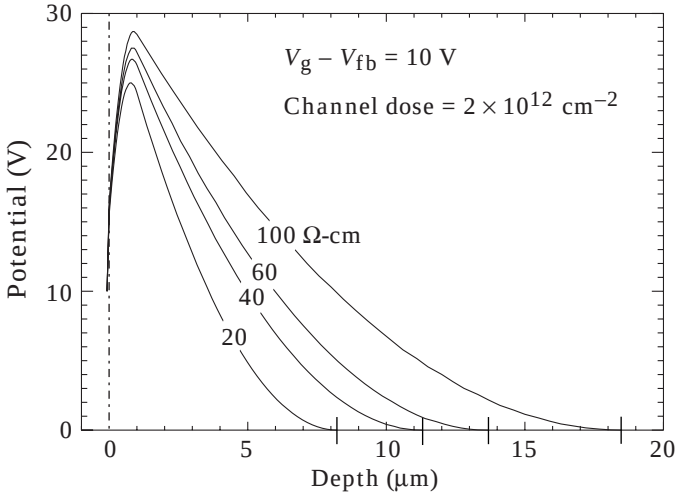

Figure 7. Potential as a function of depth for typical epitaxial layer resitivities. The channel dose is $2 \times 10^{12}\,\mathrm{cm}^{-2}$, and $V_g - V_{fb} = 10$ V. Other parameters (channel thickness, substrate doping, etc.) have typical values. Note the variation of the field-free region thickness with resistivity. Calculations are by S. E. Holland.

This is true for any non-depleted CCD. For example, MIT/LL uses a high-resistivity substrate to obtain a 40 μm sensitive region, enhancing the red sensitivity without incurring an unacceptably thick field-free region.

The UC/LBNL approach is to overdeplete the entire active region (the wafer thickness, about 300 μm) by application of an external biasing potential.[17] Under these conditions there is then no field-free region, but in return for the thickness lateral diffusion in the depleted region must be considered. Theoretical expectations and experimental measurements of the rms projected PSF width are shown in the left side of Fig. 8.[15] Measurements were made on images obtained by illuminating a CCD with 15 μm pixels through a mask containing an array of small pinholes. The results are high because of undersampling, but we can conclude that the intrinsic width of the PSF is 7–8 μm at moderate bias voltages. The width scales as $\approx 1/\sqrt{V_{\mathrm{bias}}}$, so there is no great advantage to higher bias voltages. It also scales as the wafer thickness, but a thinner chip would have decreased near-IR response.

Measuring the thickness of the field-free region in a thinned CCD is tricky. One approach is to analyze the tracks left by very oblique cosmic ray muons, where a "blob" at one end of the track is due to field-free diffusion. This is illustrated in the right half of Fig. 8, using a CCD like that used for the PSF measurements. For $V_{\mathrm{bias}} = 10$ V, 7–8 V below depletion voltage, it is evident that about 1/3, or ≈ 100 μm, is field-free. In the 30 V case there is no "blob," but diffusion of the charge transported the greatest distance is still evident. A quantitative analysis of cosmic ray tracks provides an alternative way to measure the PSF; results have been in good agreement with the pinhole mask method.[18] Alternatively, the field-free thickness can be extracted from a measured MTF.

5. ORTHOGONAL TRANSFER CCDS

The orthogonal transfer CCD (OTCCD) is an exceedingly important and interesting development, although not (yet) on the main track of the evolution discussed above. It is being developed by J. L. Tonry in collaboration with B. E. Burke and others at MIT/LL, and the operation of a 64×64 pixel device was described in 1994.[19] Two 1997 papers[7,8] described engineering and science results using a 512×512 device.

In a normal CCD the charge is clocked along columns, with channel stops preventing charge transport in the orthogonal direction (rows). A repeated 3-gate structure perpendicular to the columns facilities the charge transfer without losing the integrity of the charge collected in each pixel. The Tonry/Burke idea was to replace the channel stop with a 4th gate, so that charge could just as easily be transported in either direction. The idea, as explained in the 1997 papers, is that if gate 4 is held low, the sequence 1–2–3–1 high would transfer charge in one direction along a "column," and 1–3–2–1 would transfer charge in the opposite direction, as usual. But if 1 were held low, then 1–4–2–1 and 1–2–4–1 high would move charge in the positive and negative directions along the "row" direction.

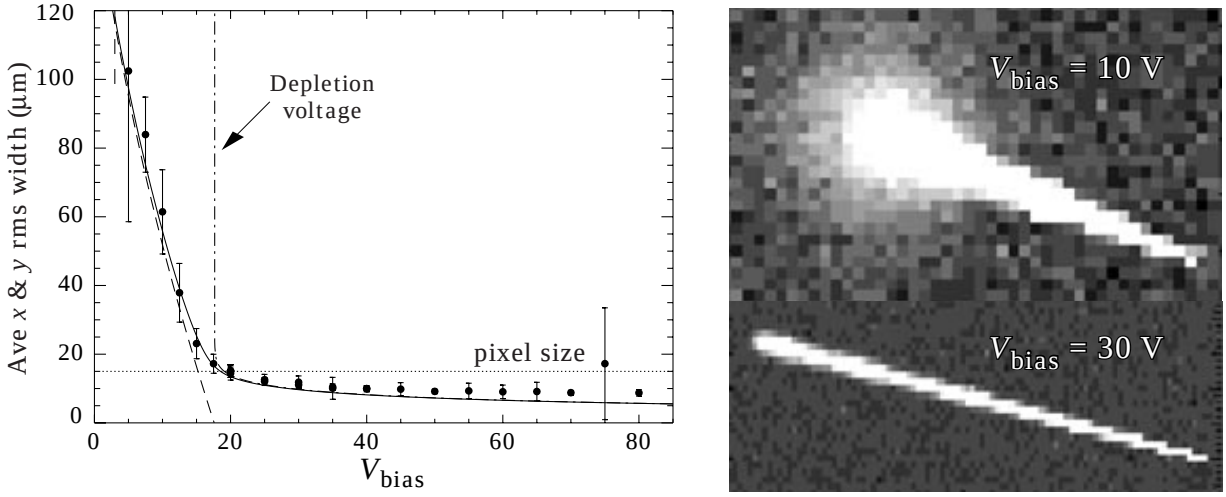

Figure 8. (left) Experimental measurements of projected PSF rms width, compared with theory, as a function of bias voltage $V_{\rm bias}$;[15] (right) Cosmic ray muons, showing effect of undepleted region.

Channel stop "spots" at the corners of the of the pixels prevent leakage into corner-touching potential wells while clocking. With this arrangement the CCD is totally symmetric with respect to rows and columns.

Two different geometries have been developed to implement this scheme.[9,20] A photomicrograph of the first, with pixels outlined by linear gates 1 and 4 and with triangular gates 2 and 3, is shown in Fig. 9(a). A cartoon of the newer, more symmetric design is shown in Fig. 9(b). Gates all have the same mowing-machine blade design shown schematically in Fig. 9(c), with the narrow segments crossing in the channel stop spots. The (repeated) gate numbering scheme used is shown in both cases for one pixel.

In an ordinary CCD there is nothing special that defines the gate that should be held high during the collection phase, nor is there any reason to choose potential wells 1/3 pixel removed. But in this case, where one is shifting charge around in response to some local tracking requirement, there is no longer any reason to define a pixel at a fixed 3-gate-wide location. Shifts can just as easily be by 1/3 pixel, making the minimum shift 5 μm in the case of 15 μm "pixels."

The development was driven by the desire to shift charge around quickly in two dimensions in response to atmospheric-induced image motion or telescope motion irregularities. The use of an array of 600×600 pixel, some fraction of which become guide-star followers, has been described about with regard to the WFHRI proposal.[9]

In an ordinary CCD the choice of which gate to hold high during the collection phase is arbitrary, and there is no particular reason to shift by 1/3 pixel during an exposure. But in this case, where one is shifting charge around in response to some local tracking requirement, there is no longer motivation to define a pixel at any fixed 3-gate-wide location. The quantum of shift thus becomes 1/3 pixel, making the minimum shift 5 μm in the case of 15 μm "pixels," or, in the case of the proposed WFHRI detectors, 1/3 of the 5 μm pixels.

The obvious problem with this scheme is that charge must be moved thousands of times, tremendously exacerbating sensitivity to charge transfer efficiency and, especially, to charge traps (pockets), which temporarily store charge for later release. The 1997 papers discussed this problem in some detail, along with potential possible solutions. The CTE problem was at the 1% level, and was judged acceptable. It is now understood that the use of aluminum for the 4th gate in these first OTCCDs, deposited as part of the same step as was used to deposit bonding pads and interconnections, was responsible for the problem.[20] The use of polysilicon for the 4th gate, as well as for the other three, seems to have virtually eliminated the problem.

6. CCDS FOR ADAPTIVE OPTICS

In the early 1950's Horace Babcock suggested an adaptive optics (AO) instrument which could regain the resolution lost to atmospheric turbulence.[21] Its implementation was well beyond the technology of his time. Even when such

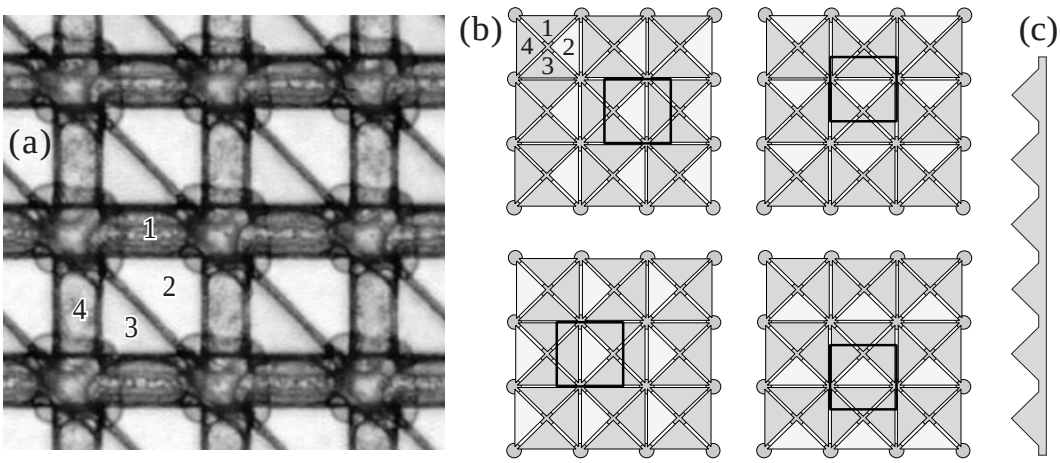

Figure 9. (a) Photomicrograph of Type 1 OTCCD, showing the gate arrangement.[7,8] (b) Cartoon of the symmetric Type 2 OTCCD. Light gates are "high," and the dark squares indicate charge centroids differing by 1/3 pixel..[9,20] (c) Schematic of the Type 2 gate profile. Photomicrograph and other material courtesy of B. E. Burke, MIT/LL.

an instrument became practical, the low probability of a bright guide star near an an arbitrary object of interest was daunting. In the 1980's several developments changed astronomers' perception: Infrared (IR) arrays became available; it was realized that the AO requirements in the IR were less stringent; optical guidestars could be used to sense the corrections for IR wavelengths; and, finally, Foy and Labeyrie suggested the use of laser guide stars.[22] By the mid-1990's, more than 20 astronomical AO systems were operating or under construction.[23]

In the usual AO system, an image of the telescope's exit pupil (mirror) is reflected from a deformable mirror—a thin mirror whose figure is controlled by a large number of piezoelectric actuators (> 200 and rising by the year). Part of the light from a subsequent beam splitter goes to the science detector, while the rest goes to a wavefront sensor. In one scheme a (Shack-Hartmann) array of "lenslets" focuses an array of guidestar images onto a CCD. Typically each image is focused onto four pixels, and the corners between the subarrays correspond to actuator positions on the deformable mirror.[24] This arrangement is shown in Fig. 10; in this case there are 241 actuators inside the exit pupil (shown in gray), and a 32×32 CCD is needed.

The characteristics of the required CCD are easy to list:

- It is difficult to fabricate the lenslet array with elements much smaller than 200 μm, so that even with the use of an additional lens large pixels are desirable. However, all of the mechanisms responsible for charge transfer without excessive loss have time constants which increase with pixel size.[25] Fast readout thus constrains pixel size, and a 24 μ pixel compromise is typical for available devices.

- The number of pixels is defined by the requirement that there is one subarray for each actuator inside the exit pupil. For the present generation of infrared AO at the 8–10 m telescopes, 64^2 is sufficient, but one can envisage future needs for 256^2 pixels.[26]

- The time scale for readjusting the optics is set by the time it takes the wind, with velocity v, to move across a turbulent cell whose size is characterized by the Fried parameter r_0. Under average observatory conditions r_0/v is about 30 ms for visible light. r_0 scales approximately as $\lambda^{1.2}$, so the time scale is somewhat longer in the IR. In any case, the corrections must be made at least several hundred times per second, and possibly more. The minimum requirement is thus for a CCD with a frame rate of 1000 frames/s; 1500 frames/s would be better.

- The number of available guidestars increases rapidly when fainter and fainter stars can be used, so there is a great premium on determining the centroid in the subarray using as few photons as possible. This, in turn, requires very low read noise—a demand somewhat at variance with the requirement for speed. For example, the PixelVision Adapt3, an 80×80 CCD with $(36\ \mu\text{m})^2$ pixels, obtains 4 e^- noise at 250 frames/s, but only 12 e^- at 1250 frames/s.[27]

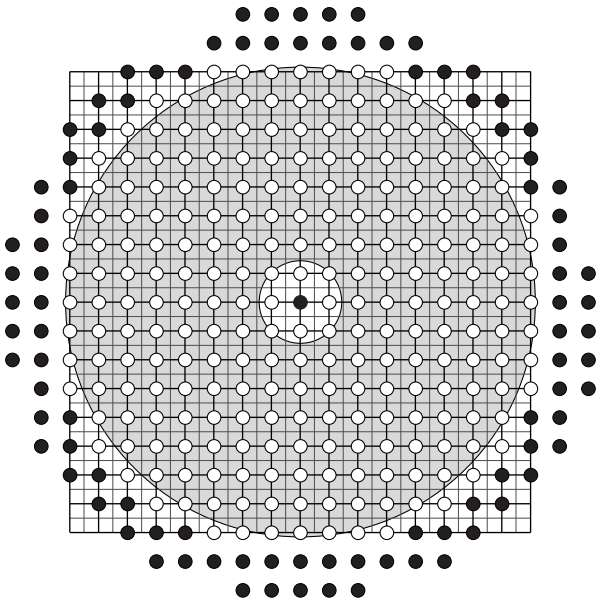

Figure 10. Schematic showing the mapping of actuators and telescope exit pupil (mirror, in grey) onto the wavefront sensing CCD. Actuators map to the corners of 4-element subarrays in this example. Active actuators are shown in white; support actuators, which determine the "boundary conditions," are in black.

Fast readout and low noise are facilitated by a large number of outputs. For example, the MAT CCD50 has 16.

- There are a lot more red stars than blue stars, so there is a premium on good red response. A CCD with a thick sensitive region is desirable.

Adaptive optics CCDs are being supplied by a number of manufacturers, and considerable development is in progress. For example, the MIT/LL CCID19 has 64^2 $(21\ \mu\mathrm{m})^2$ pixels read out by 4 ports, and achieves 5–6 e^- read noise at speeds up to 500 frames/s. It has a high-resistivity substrate and thus extended red response. CCDs with double this speed and 3–4(?) e^- read noise are promised for next year (2000). A 128^2 pixel fast-readout CCD with 16 ports is under development.[26]

The MAT CCD50, with 128^2 $(24\ \mu\mathrm{m})^2$ pixels, can be read out (16 outputs) at 1 kHz with ≈ 6 e^- noise. About 2 e^- can be achieved with slower readout. Its replacement, the CCD60, has the same format but only one output, and is expected to achieve ≤ 2 e^- noise at about 1000 frames/s.[14]

We have already mentioned the PixelVision AO CCD.[27] Rockwell supplies an IR-sensitive array.[26]

This list is not intended to be comprehensive, but rather to indicate the present rather impressive capabilities and the expected improvements.

7. OTHER SUBJECTS

The cost of the highly coveted observing time at large telescopes is hard to estimate, but it is certainly in excess of $10,000 per night, or about $20 per minute. The cost difference between a 2 min and a 30 s array readout time can thus easily exceed $1500 per night, even with moderately long exposures. This accumulated overhead expense approaches the cost of the CCD camera in a few years, or about the lifetime of a typical camera. There is obviously a great premium on parallel readout of all the CCDs in an array, through more than one output per CCD. Other overhead not associated with readout time also increases deadtime. The details are beyond the scope of this paper, but effort is going into decreasing the lost time.

The sky imaged by a large array will inevitably have a number of bright stars in even carefully chosen fields, resulting in lost imaging area and inaccessible parts of the field due to blooming. Several antiblooming techniques have been and are being developed, but again the details will not be covered here.

This paper has presented an overview of selected subjects in a vibrant and exciting field. There is much in store.

ACKNOWLEDGMENTS

I am indebted to a very large number of people who sent me material, answered my questions, and otherwise tried to educate me. First and foremost of these is Steve Holland. Barry Burke, Jim Janesick, Paul Jordan, Jerry Nelson, and, especially, Gerry Luppino were helpful and patient. Communications with a large number of mosaic builders and others were invaluable. My partial understanding has very likely led to errors which are in no wise the fault of my sources. This work was supported by the U.S. Department of Energy under contract No. DE-AC03-76SF00098, and by the National Science Foundation (US) under grant NSF/ATI 9876605.

REFERENCES

1. R. Florence, *The Perfect Machine*, Harper, 1997.
2. J. R. Janesick, *Scientific Charge Coupled Devices*, SPIE Press (to be published).
3. D. F. Edwards, "Silicon (Si)," in *Handbook of Optical Constants of Solids*, E. D. Palik, ed., pp. 547–569, Academic Press, 1985.
4. J. R. Janesick, "Advanced applications of scientific charge coupled devices," *IS&T/SPIE Symposium on Electronic Imaging Science and Technology* , p. 233, (no data source or year given).
5. K. Rajkanan, R. Singh, and J. Shewchun, "Absorption coefficient of silicon for solar cell calculations," *Solid-State Electronics* **22**, pp. 793–795, 1979.
6. D. E. Groom, S. E. Holland, M. E. Levi, N. P. Palaio, S. Perlmutter, R. J. Stover, and M. Wei, *SPIE* **3649**, 80–90, 1999.
7. B. E. Burke & J. L. Tonry, *SPIE* **3019**, 233–240, 1997.
8. J. L. Tonry, B. E. Burke, & P. L. Schechter, *Proc. Astron. Soc. Pacific*, **109**, 1154-1164, 1997.
9. N. Kaiser, J. L. Tonry, & G. A. Luppino, `astro-ph/9912181`, to be published in *Proc. Astron. Soc. Pacific* (2000).
10. O. Saint-Pé, *Proc. 4th ESO Workshop on Optical Detectors for Astronomy*, Garching, Germany, 13–16 September 1999 (to be published, 2000), and O. Saint-Pé, private commu*Proc. Astron. Soc. Pacific.*
11. M. Lesser, D. Ouellete, A.J. P. Theuwissen, K. L. Kreider, & H. Michaelis, IEEE, "Packaging and Operation of Philips 7k×9k CCDs," Workshop on CCDs and Advanced Imaging Sensors in Brugge, Belgium (1997), available at `http://sauron.as.arizona.edu/`.
12. D. Wen, R. Bredthauler, P. Bates, P. Vy & R. Potter, pp 171–174, Proc. 1999 IEEE Workshop on Charge-Coupled Devices and Advanced Image Sensors, June 10-12, Karuizawa, Nagano, Japan.
13. M. M. Blouke & B. Corrie, *Proc. 4th ESO Workshop on Optical Detectors for Astronomy*, Garching, Germany, 13–16 September 1999 (to be published, 2000).
14. P. R. Jorden, Peter Pool, & Ralph Holtom, "Latest EEV CCD developments, and technologies for scientific CCDs," *Proc. 4th ESO Workshop on Optical Detectors for Astronomy*, Garching, Germany, 13–16 September 1999 (to be published, 2000).
15. D. E. Groom, P. H. Eberhard, S. E. Holland, M. E. Levi, N. P. Palaio, S. Perlmutter, R. J. Stover, and M. Wei, "Point-spread function in depleted and partially depleted CCDs," *Proc. 4th ESO Workshop on Optical Detectors for Astronomy*, Garching, Germany, 13–16 September 1999 (to be published, 2000).
16. P. H. Eberhard & S. E. Holland, private communications 1999–2000; also see above reference.
17. S. E. Holland, G. Goldhaber, D. E. Groom, W. W. Moses, C. R. Pennypacker, S. Perlmutter, N. W. Wang, R. J. Stover, and M. Wei, IEDM Tech. Digest, 911 (1996).
18. B. Hodges (Lawrence Berkeley National Laboratory, unpublished, 1999).
19. B. E. Burke, R. K. Reich, E. D. Savoye, & J. L. Tonry, IEEE Trans. Electron Devices **41**, 2492 (1994).
20. B. E. Burke et al., "CCD Imager Technology Developments at Lincoln Laboratory," *Proc. 4th ESO Workshop on Optical Detectors for Astronomy*, Garching, Germany, 13–16 September 1999 (to be published, 2000).
21. H. W. Babcock, Publ. Astron. Soc. Pac. **65**, 229 (1953).
22. R. Foy & A. Labeyrie, Astron. Astrophys. **152**, L29 (1985).
23. L. A. Thompson, Physics Today, Dec. 1994, p. 24.
24. M. C. Roggemann, B. M. Welsh, & R. Q. Fugate, Rev. Mod. Phys. **69**, 437–505 (1997).
25. J. Janesick, J. Pinter, & J. McCarthy, "High speed scientific CCDs–II," to be published.
26. J. Beletic, Center for Adaptive Optics Workshop, Santa Cruz, CA, 22–23 November, 1999.
27. `http://www.pvinc.com/adapt3-main.htm`